Visible Light-Driven Selective Organic Degradation by $FeTiO_3$/Persulfate System: the Formation and Effect of High Valent Fe(IV)

Lihan Pan[†], *Wen Shi*[†], *Tapas Sen*[‡], *Lingzhi Wang*[†,*], *Jinlong Zhang*[†,*]

[†]Key Lab for Advanced Materials and Joint International Research Laboratory of Precision Chemistry and Molecular Engineering, Feringa Nobel Prize Scientist Joint Research Center, Institute of Fine Chemicals, School of Chemistry and Molecular Engineering, East China University of Science & Technology, 130 Meilong Road, Shanghai, 200237, China.

[‡]School of Physical Sciences & Computing, Centre of Materials Sciences, University of Centr al Lancashire, Preston, UK.

Corresponding author: Lingzhi Wang and Jinlong Zhang

Key Lab for Advanced Materials and Joint International Research Laboratory of Precision Chemistry and Molecular Engineering,

East China University of Science and Technology, Shanghai 200237, P.R. China

Tel & Fax: +86-21-64252062.

E-mail: wlz@ecust.edu.cn; jlzhang@ecust.edu.cn

Abstract

The role of high-valent Fe has rarely been explored in persulfate-based heterogeneous reaction. Herein, the existence of Fe(IV) is verified in a visible light-assisted $FeTiO_3$/persulfate system using methyl phenyl sulfoxide as the probe. The $FeTiO_3$/persulfate/light system is capable of selectively degrading aromatic compounds with a higher ionization potential including tetracycline and bisphenol A by photo-generated high-valent Fe(IV). The contributions from $SO_4^{\cdot-}$, $^{\cdot}OH$ and $^1O_2$ are excluded. The comparable efficiency in the dark requires higher dosages and suffers from a rapid deactivation. Based on XPS, Raman and EPR analyses, the poor dark activity is caused by the formation of a complex between *in situ* formed Fe(III) and SO_4^{2-} on the $FeTiO_3$ surface; this complex is, however, the key intermediate for Fe(IV) production under the light irradiation. This study reveals the long-ignored role of SO_4^{2-} as an abundant species in iron-based persulfate systems. We also call for re-evaluating the real oxidation mechanism in other persulfate-based reactions considering the different oxidation mechanisms of radicals and high-valent iron.

Keywords

$FeTiO_3$; persulfate; high valent Fe(IV); irradiation; selective degradation

This manuscript is dedicated to, and in memory of, the late Prof. Maria Flytzani

1. Introduction

Fenton and Fenton-like reactions in advanced oxidation processes (AOPs) have received intense attention for the elimination of recalcitrant pollutant through the generation of aggressive species such as the hydroxyl ($^{\cdot}OH$), superoxide ($O_2^{\cdot-}$) and sulfate ($SO_4^{\cdot-}$) radicals.[1] Iron-based species (simplified as Fes) are the most commonly used catalysts in both homogeneous and heterogeneous systems.[2-7] For the Fes/H_2O_2 system, there was a long-standing argument about the role of the high-valent Fe(IV) and $^{\cdot}OH$ as the active species. The contribution from Fe(IV) in acidic environment was finally excluded by Bakac et al using dimethyl sulfoxide (DMSO) as the probe.[8] Later, it was confirmed that Fe(IV) is the active species at neutral pH.[9] Similar to $^{\cdot}OH$ generation from Fes/H_2O_2,[10-13] the activation of persulfate ($S_2O_8^{2-}$, PS) by Fes is one of the most popular approaches for producing $SO_4^{\cdot-}$ radical that has a higher oxidizing power (E^0 = 2.5−3.1 V vs NHE) comparable to that of $^{\cdot}OH$ (E^0 = 2.8 V vs NHE) and a longer lifetime (300 μs) than $^{\cdot}OH$ (40 μs).[14-18] It is commonly observed that $SO_4^{\cdot-}$ can be further evolved into $^{\cdot}OH$, particularly in basic conditions and both of these radicals can be the active species for organic degradation.[19-23] The contribution of $SO_4^{\cdot-}$ rather than that of $^{\cdot}OH$ to organic degradation is usually identified through the alcohol scavenging strategy since $^{\cdot}OH$ shows similar reactivity toward EtOH and tert-butyl alcohol (TBA) while $SO_4^{\cdot-}$ shows higher reactivity toward EtOH.[24] In contrast, Jiang et al. recently verified the existence of Fe(IV) in a homogeneous Fe^{2+}/PS system using methyl phenyl sulfoxide (PMSO) as the probe.[25] They doubted that the different alcohol scavenging effect could be attributed to the higher reactivity of Fe(IV) for EtOH instead of TBA and claimed that Fe(IV) rather than $SO_4^{\cdot-}$ should be the real active species toward organic degradation.

The oxidation process by Fe(IV) is achieved mainly by oxygen/hydrogen atom transfer,[26-28] which could result in a better selectivity towards organic degradation compared with the more aggresive $SO_4^{\cdot-}$ or $^{\cdot}OH$. The verification of Fe(IV) in the homogeneous PS-based system may lift the curtain on study about the possible role of Fe(IV) for organic degradation in

versatile Fes-containing systems. The heterogeneous reaction benefits from good separability, wide availability of Fe ore in nature and flexible utilization of light or electricity.[29] The reaction on the catalyst surface may lead to a different redox path compared with that in homogeneous reation.[30] It is thus highly urgent to explore the relation between PS decomposition and the formation of Fe(IV) in the heterogeneous reaction considering the different redox characteristics of Fe(IV) and $SO_4^{\cdot-}$.

Iron and titanium oxides are abundant in nature and show low biotoxicity. Herein, $FeTiO_3$ as the main component of ilmenite with a band gap of 2.4-2.9 eV is used for the activation of PS under dark conditions ($FeTiO_3$/PS/dark) and the visible light irradiation ($FeTiO_3$/PS/light). Selective and stable degradation to phenolic compounds with higher ionization potential was achieved in the $FeTiO_3$/PS/light system, while nonselective degradation and rapid deactivation were observed in the $FeTiO_3$/PS/dark system. The contribution from Fe(III)-SO_4 complex on the $FeTiO_3$ surface to the formation of Fe(IV) and the role of Fe(IV) as the active species in the selective organic degradation were verified through the combination of EPR, XPS and ^{1}H NMR analyses.

2. Experimental Section

2.1 Chemicals and Materials

Titanium isopropoxide (TTIP), tetrabutylammonium hydroxide (TBAH, 10%), ferrous sulfate heptahydrate ($FeSO_4 \cdot 7H_2O$), potassium hydroxide (KOH), potassium persulfate ($K_2S_2O_8$), potassium iodide (KI), sodium acetate (NaAc), acetic acid (HAc), 2, 4-dichlorophen (2, 4-DCP) and hydrogen peroxide (H_2O_2, 30%) were purchased from Sinopharm Chemical Reagent Co., Ltd., China. Tetracycline hydrochloride (TC), terephthalic acid (TPA), bisphenol A (BPA) and dimethyl sulfoxide (DMSO) were obtained from Aladdin Co. Methyl phenyl sulfone ($PMSO_2$) and methyl phenyl sulfoxide (PMSO) were purchased from Macklin. All of the reagents used in this work were at least analytical grade and ultrapure water was used for all experiments.

2.2 Preparation of Catalyst

The $FeTiO_3$ catalyst was fabricated using a simple solvothermal method reported previously.[31] Briefly, TTIP (0.6 mL) was added to a mixture of TBAH (5 mL) and ultrapure water (10 mL) under vigorously stirring until it became clear. Then, $FeSO_4 \cdot 7H_2O$ (0.556 g) was dissolved in ultrapure water (5 mL) to form a light green solution in another beaker. The above solutions were mixed and then, the pH was adjusted to 14 using KOH. The resulting suspension was transferred to a Teflon-lined stainless steel autoclaves and placed in an oven at 220 ^{0}C for 12 h. The obtained products were washed with water and ethanol and dried prior to use.

2.3 Characterization

The crystal phases of the as-prepared samples were analyzed by XRD conducted in order to identify the samples' microstructure characteristics. The XRD data were collected in the range of 5-80° (2θ) and recorded on a Rigaku D/MAX-2550 diffractometer using Cu Kα radiation with the wavelength of 1.5406 Å, typically operating at a voltage of 40 kV and current of 100 mA. Transmission electron microscopy (TEM) was conducted with a JEOL JEM-2100EX electron microscope, using an accelerating voltage of 200 kV. Raman measurements were performed at room temperature using a Via + Reflex Raman spectrometer with the excitation wavelength of 532 nm. The BET surface area of the sample was determined by nitrogen adsorption at 77 K (Micromeritics ASAP2010). The sample was degassed at 373 K prior to the measurement. TC values were monitored using a SHIMADZU SPD-M20A reverse-phase high-performance liquid chromatography (HPLC) system at a flow rate of 1 mL·min^{-1} with a RX-C18 column (4.6 × 250 mm, 5 μm) and a diode array UV-vis detector (356 nm). The mobile phase A was composed of 0.01 M oxalic acid, while mobile phase B was pure acetonitrile, and the ration of A to B is 4:1. The leaching concentration of Fe was calculated using an inductively coupled plasma-atomic emissions spectrometer (ICP-AES, Vanan 710).

The detection of radicals and EPR spectrum are recorded on 100G-18KG/EMX-8/2.7 Electro-Spin Resonance Spectrometer.

2.4 Organic Degradation

Organic stock solutions with high concentration were prepared. Aliquots of the stock solutions were combined to achieve the initial experimental conditions. All of the reactions were carried out at room temperature under exposure to air. The light source was a 300 W Xe lamp equipped with wavelength cut off filters ($\lambda \geq 420$ nm) and the reactor vessel was placed 12 cm away from the lamp. The optical power is 570 mW and the optical density is 697 mW/cm^2. A certain amount of the catalyst was firstly mixed with organics solution and stirred in the dark for 30 min to achieve the adsorption/desorption equilibrium. The experiments commenced by injecting PS into the solution. During the degradation process, an appropriate amount of the turbid solution was immediately withdrawn from the above solution with syringes at fixed time intervals and filtered with 0.22 μm polytetrafluoroethylene syringe filters and it was observed that the filtration had no obvious impact on the organic concentration. The clear liquid was immediately analyzed by HPLC. Organic degradation in the dark was carried out in a similar manner except for the absence of light irradiation. All of the experiments were performed at least 3 times; with the error bars in figures representing the standard deviation. For the TC degradation carried out in buffer solution, the pH was maintained at 4 by adding 5 mL buffer solution, which consists of 75 mM sodium acetate and 125 mM acetic acid. The buffer of 8 and 10 were composed of 10 mM Borate/25 mM phosphate and 12.5 mM Borate/40 mM sodium hydroxide, respectively. After the reaction, the pH difference was no more than 0.2, which show that pH buffers have excellent stability.

2.5 Stability and Reusability

To test the stability and reusability of FeTiO3/PS/light and FeTiO3/PS/dark systems, the catalyst was washed with methanol and ultrapure water several times after each cycle and

158 then was immediately applied for the next cycle. Mixed cycle performance was conducted by
159 applying the catalyst used 5 times in the dark for the light irradiation system.

160 **3. Results and Discussion**

161 **3.1. Structure of $FeTiO_3$**

162 Figures 1a and 1b are the TEM and SEM images of the prepared $FeTiO_3$ particles, which
163 have a hexagonal plate-like structure with a side length of ca. 800 nm and a thickness of ca.
164 50 nm. The XRD patterns of the as-prepared $FeTiO_3$ are shown in Figure 1c. The peaks at 2θ
165 of 23.8º, 32.5º, 35.3º, 40.3º, 48.7º, 53.0º, 61.5º and 63.3º agree well with the ilmenite $FeTiO_3$
166 structure (JCPDS Card No. 29-0733). The sharp peaks demonstrate the high crystallinity of
167 $FeTiO_3$.

168 **3.2. Fe(IV) and Radical Species**

169 Currently, it remains unclear whether Fe(IV) is generated through activating PS in the
170 heterogeneous iron-containing system, where $SO_4^{\cdot-}$ or $^{\cdot}OH$ hydrolyzed from $SO_4^{\cdot-}$ has long been
171 recognized as the dominant reactive species for organic degradation. Here, the formation of
172 Fe(IV) in the $FeTiO_3$/PS/light system is explored using PMSO as the probe, which as a
173 sulfoxide can be oxidized to the corresponding sulfones by Fe(IV) through an oxygen atom
174 transfer step. According to the HPLC analysis (**Figures 2**a, S1, Table S1), $PMSO_2$ can be
175 detected under the visible light irradiation, but is absent in the dark. The reacted PMSO
176 molecules are almost completely transformed to $PMSO_2$ according to the formation efficiency
177 of $\eta(PMSO_2)$ (Figure S1), demonstrating the formation of Fe(IV) species. Mossbauer
178 spectroscopy was further adopted to confirm the existence of the Fe(IV) species. According to
179 the Mossbauer spectrum of the $FeTiO_3$ after the light irradiation in the presence of PS (Figure
180 2b), ca. 42% of Fe(II) is oxidized, among which 4.5% is attributed to Fe(IV). Besides, EPR
181 tests were further performed using DMPO as a radical spin trapping agent to understand the
182 formation and evolution of possible radical species in different $FeTiO_3$/PS systems. As

observed from Figure 2c, the $FeTiO_3$/PS/dark system shows negligible signal attributed to DMPO-$SO_4^{\cdot-}$, indicating the poor ability of $FeTiO_3$ to activate PS under dark conditions. By contrast, the $FeTiO_3$/PS/light system presents distinct signals attributed to DMPO-$^{\cdot}OH$.[32] The $^{\cdot}OH$ radical is possibly formed from the hydrolysis of $SO_4^{\cdot-}$or the oxidation of OH^-/H_2O by photo-generated hole according to the previous reports.[33-36] Moreover, the existence of singlet oxygen ($^1O_2$) is also verified using TEMP as the probe (Figure 2d).

3.3. Organic Degradation

The organic degradation performance of the $FeTiO_3$/PS/light system was evaluated using tetracycline hydrochloride (TC), bisphenol A (BPA), terephthalic acid (TPA) and 2, 4-dichlorophenol (2, 4-DCP) as the pollutant models. As shown in **Figure 3**a, only ca. 20% of TPA is degraded within 1 h in the presence of 0.10 g/L of $FeTiO_3$. 2, 4-DCP is removed with a moderate efficiency of ca. 50%. It is noted over 80% of BPA is degraded and the complete elimination of TC is achieved within 1 h. In comparison, no selective oxidation was observed in the UV/PS system (Figure S2). Moreover, all the organics are recalcitrant to degradation under dark conditions (Figure 3b). The photocatalysis by $FeTiO_3$ can be excluded according to the low efficiency of ca. 19% toward TC elimination under the visible light irradiation in the absence of PS (Figure S3a). Meanwhile, the substitution of H_2O_2 to PS leads to a negligible removal of TC regardless of whether the light irradiation is used (Figure S3b), demonstrating the essential role of PS for the degradation. It seems the degradation performance of the $FeTiO_3$/PS/light system is strongly correlated with the ionization potential (IP) of the organics. Specifically, TC and BPA with electron-donating groups such as hydroxyl and amido usually have lower IP values, which are more readily to be degraded, whereas TPA and 2,4-DCP with electron-withdrawing carboxyl and halogen atom are less prone to degradation.[37, 38]

The influences of the PS concentration and catalyst dosage in the $FeTiO_3$/PS/light system were further investigated over TC, where ca. 80% of TC can still be degraded when the PS

concentration decreases form 2 mM to 1 mM (Figure S4a). The apparent rate constant for the degradation of TC with 1 mM of PS is calculated as 9.60 (**Equation 1**, Figure S4). Moreover, the interference from pH variation during the degradation is excluded according to the preserved activity in the pH buffering solution (pH = 4, Figure 3c); The effect of homogenous reaction by leached iron (0.028 $mg \cdot L^{-1}$ after 1h) is also denied based on the control experiments in the homogeneous Fe^{2+} or Fe^{3+} system (Figure S3c).[39, 40]

$$V = dc/dt = 9.60[K_2S_2O_8]^{0.9667} [FeTiO_3]^{1.6667} \quad (1)$$

3.4. Identifying the Active Species

As demonstrated above, there are radicals including $^{\cdot}OH$, $SO_4^{\cdot-}$ and $^1O_2$ besides Fe (IV) in the $FeTiO_3$/PS/light system, which are all possible reactive species for the organic degradation. Taking TC degradation as the model, radical quenching experiments were carried out to identify the real reactive species in the $FeTiO_3$/PS/light system. EtOH and TBA are the most commonly used alcohol scavengers due to their different reactivity with the $SO_4^{\cdot-}$ and $^{\cdot}OH$ radicals (EtOH for both $SO_4^{\cdot-}$ and $^{\cdot}OH$, TBA for $^{\cdot}OH$, Table S2).[25] The concentrations of scavengers are 100 times higher than that of PS in order to ensure the full quenching effect. **Figure 4** shows that the presences of EtOH and TBA decrease the removal efficiency to ca. 25% and 52%, respectively. This result is generally used to demonstrate that $SO_4^{\cdot-}$ radicals are the main species for the organic degradation; however, this is inconsistent with the EPR analyses considering the strong DMPO-$^{\cdot}OH$ and negligible DMPO-$SO_4^{\cdot-}$ signals. Moreover, it is doubtful that the hydrolysis of $SO_4^{\cdot-}$could lead to the complete disappearance of the DMPO-$SO_4^{\cdot-}$signal in ERP spectrum considering the low reaction kinetics in acidic conditions (**Equation 2**),[41, 42] which suggests that DMPO-$^{\cdot}OH$ adduct may be not formed from $^{\cdot}OH$ radical. It was recently reported by Jiang et al that the more severe activity-inhibition by EtOH could be ascribed to the higher reaction kinetics of Fe(IV) toward EtOH (2.51×10^3 M^{-1} s^{-1}) than TBA (6.0×10^1 M^{-1} s^{-1}, Table S2).[25] Therefore, it is highly possible the

strong EPR signal of the DMPO-$OH^{\cdot}$ adduct under the acidic conditions may be due to the direct oxidation of DMPO by Fe(IV) in the similar manner revealed from Mn(VII) (**Scheme 1**).[41, 43, 44]

$$SO_4^{\bullet-} + H_2O \rightarrow SO_4^{2-} + OH^{\bullet} + H^+ \quad k = 2.0 \times 10^{-3}\ M^{-1}s^{-1} \qquad (2)$$

DMSO was further used to exclude the possible contribution from $^{\cdot}OH$.[45] Similar to the situation for PMSO, Fe(IV) is capable of oxidizing DMSO to $DMSO_2$ through oxygen transfer, while $^{\cdot}OH$ generates methyl sulfinic acid ($DMSO_3H$) through a completely different path.[46] The presence of DMSO in $FeTiO_3$/PS/light system causes an adverse effect on TC degradation (Figure 4a). According to the ^1H NMR spectrum, only the peak of $DMSO_2$ can be clearly observed besides the strongest peak of DMSO.[47] The absence of signal attributed to methyl sulfinic acid confirms the adverse effect for TC degradation by DMSO should be related to the consumption of Fe(IV) instead of $^{\cdot}OH$ radical (Figure 4b, inset).

Regarding the possible contribution from $^1O_2$, $FeTiO_3$/H_2O_2/light was adopted as a control system which presents distinct EPR signals attributed to the ring-opening product oxidized from $^1O_2$, similar to that observed from the $FeTiO_3$/PS/light system (Figure S5).[32] However, the low activity of the H_2O_2 system suggests that $^1O_2$ is not the active species for TC degradation. It is also found that the system with tryptophan, which is a commonly used capture agent for $^1O_2$, had little effect on the degradation performance (Figure 4a), thus further excluding the role of $^1O_2$ as the reactive species. The above results well suggest the selective degradation of aromatic compound with higher IP should be achieved via the formation of high-valent Fe (IV) species on the $FeTiO_3$ surface.

3.5. Degradation Stability

Using the $FeTiO_3$/PS/dark system with 1 mM PS as the illustration, $FeTiO_3$/PS/light system well maintains the degradation activity toward TC for 5 cycles (**Figure 5**a). Considering the inevitable mass loss during the recycling operation, the $FeTiO_3$/PS/light system is very efficient and stable in each cycle. The simultaneous increases of the PS (5 mM) and $FeTiO_3$

(0.2 g/L) concentrations under dark conditions can achieve reaction kinetics (**Equation 3**) comparable to that in the $FeTiO_3$/PS/light system with less agent dosage (1 mM PS + 0.1 g/L $FeTiO_3$, Figure S6). However, the degradation performance of the $FeTiO_3$/PS/dark system deteriorates rapidly during the recycling experiment, which is even reduced to 15.3% in the fifth cycle (Figure 5b), implying the vital role of the light irradiation in maintaining the degradation stability of the $FeTiO_3$/PS/light system. Moreover, it is interesting to note the deactivated sample recycled from the 5-run dark reaction shows an improved apparent rate constant (K = 16.70, **Equation 4**) compared with the fresh sample (K = 9.60, Figure 5c, Table S6). The corresponding discussion about the enhanced visible light activity of the deactivated sample will be stated in the subsequent mechanism section.

$$V = dc/dt = 10.87[K_2S_2O_8]^{1.619}\,[FeTiO_3]^{3.0333} \quad (3)$$

$$V = dc/dt = 16.70[K_2S_2O_8]^{0.9667}\,[FeTiO_3]^{1.6667} \quad (4)$$

3.6. Relation between Fe(IV) formation and PS decomposition

To understand the effect of the light irradiation on the evolution of PS and the formation of Fe(IV) species, the decomposition of PS by $FeTiO_3$ was investigated in the buffer solution (pH = 4) with and without the light irradiation. As seen from Figure S7, the decomposition efficiency is only slightly increased from the light irradiation, which re-confirms the formation of $SO_4^{\cdot-}$ from PS is not the determinative factor for the organics degradation (Equation 3). XPS analyses were used to understand the variation of Fe valence after the reaction. It is found that the percentage of Fe(III) after the light reaction is higher than that after the dark reaction (**Figure 6**a). Similar to the H_2O_2-based Fenton reaction, it is generally accepted that the oxidation of Fe(II) to Fe(III) in PS-based system is kinetically faster than the reduction of Fe(III) to Fe(II) (**Equations 5, 6**), and the light irradiation helps reduce Fe(III) to Fe(II), thus promoting the formation of $SO_4^{\cdot-}$. However, the higher Fe(III) content from the light reaction together with the insignificant EPR signal of DMPO-$SO_4^{\cdot-}$ excludes the

possibility that the enhanced activity in the $FeTiO_3$/PS/light system is attributed to the accelerated recycling of Fe(II) from Fe(III).

$$S_2O_8^{2-} + Fe(II) + H_2O \rightarrow 2H^+ + 2SO_4^{2-} + Fe(IV) \quad k = 2.0 \times 10^1\ M^{-1}s^{-1} \tag{5}$$

$$Fe(III) + S_2O_8^{2-} \rightarrow Fe(II) + S_2O_8^{\bullet-} \quad k = (6.0 \pm 0.6) \times 10^{-6}\ M^{-1}s^{-1} \tag{6}$$

$$Fe(II) + SO_4^{\bullet-} \rightarrow SO_4^{2-} + Fe(III) \quad k = 3.0 \times 10^8\ M^{-1}s^{-1} \tag{7}$$

Raman spectroscopy was adopted to explore the surface chemistry of $FeTiO_3$ before and after the reactions. It is observed that a new peak at approximately 980 cm^{-1} appears after the reaction (Figure 6b); this peak should be ascribed to the surface sulfate according to previous reports,[48-51] which is accordant with the S 2p XPS spectrum with a distinct peak at ~169 eV (Figure 6c). [30, 52, 53] The low concentration of Fe(IV) should be the reason for failing to obtain Raman signal since Raman spectroscopy is an inelastic scattering spectroscopy with low sensitivity. The theoretic calculation was further carried out to understand the sulfate adsorption on the surface of $FeTiO_3$. The (1 1 1) facet was adopted for sulfate adsorption (Figure S8). The geometry with sulfate on Fe atoms shows a more thermodynamically favorable adsorption (-226.2 kcal/mol) compared with that adsorbed on Ti atoms (-219.7 kcal/mol). Based on these results, it is conferred Fe(III) is oxidized to high-valent Fe(IV) by the photo-generated hole (**Equation 8**),[54, 55] and the remained electron is consumed by in situ formed $SO_4^{\cdot-}$ around the surface (**Equation 9**), leading to the formation of SO_4^{2-}. In this case, an efficient hole-electron charge separation can be achieved, which is accordant with the decreased photoluminescence intensity of $FeTiO_3$ in the presence of PS (Figure S9). Therefore, it is assumed that SO_4^{2-} helps stabilize the surface Fe(III) through forming ≡Fe(III)-SO_4 complex, thus increasing the Fe(III) content observed from XPS.

$$Fe(III) + h^+ \rightarrow Fe(IV) \tag{8}$$

$$SO_4^{\cdot-} + e^- \rightarrow SO_4^{2-} \tag{9}$$

3.7. Influence of pH on the Fe(IV) formation

The influence of pH on the Fe(IV) formation was further explored to understand the working pH range of the $FeTiO_3$/PS/light system. Substrate adsorption experiments proved that pH values had little effect on it (Figure S10). **Figure 7** indicates the degradation activity for TC exhibits a clear dependence on pH. Over 50% of TC can be degraded in a wide pH range of 4-10 within 1 h, except for pH of 6 where the degradation is almost completely suppressed. Since the isoelectric point of $FeTiO_3$ is approximately pH = 6, it is inferred the inhibition of the reaction is attributed to the less effective formation of the surface complex between $S_2O_8^{2-}$ and the catalyst. Under the more acidic conditions (pH = 4), $S_2O_8^{2-}$ can be electrostatically adsorbed on the $FeTiO_3$ surface and complex with Fe(II), promoting the decomposition of $S_2O_8^{2-}$. In neutral to basic conditions, $(OH)_m$-Fe(III) complex could be first formed, which also favors the transformation to Fe(IV) in the initial stage under the light irradiation. With the continuous formation of SO_4^{2-}, $(SO_4^{2-})_n(OH^-)_{m-n}$-Fe(III) is could be formed due to the greater complexing ability of SO_4^{2-} than OH^- in the presence of abundant SO_4^{2-}, further promoting the formation of surface Fe(IV) species.

3.8. Fe(IV)-induced Degradation Pathway and Mechanism

The intermediate products of TC degradation were further detected by UPLC-MS/MS to explore the Fe(IV)-induced degradation pathway. Possible reactive intermediates were listed (Table S7 and Figure S11) and the transformation pathway was proposed accordingly (Figure S12). Fe(IV) species firstly attack electron-donating groups such as amino, hydroxyl and methyl groups, leading to the formation of dihydroxylated, demethylated and deamidated intermediates, which then undergo the ring-opening for further degradation. This transformation pathway is accordant with previous reports that the oxidation process by Fe(IV) is mainly achieved by oxygen/hydrogen atom transfer.[26-28] The degradation process by Fe(IV) species is similar to the electrophilic attack by sulfate radical. The degradation

intermediates including dihydroxylated, demethylated and deamidated intermediates may also be present in reaction systems with hydroxyl or sulfate radicals.[56-60] However, since the contribution of sulfate radical and its derivative of hydroxyl radical has been excluded in $FeTiO_3$/PS/light system, the degradation of TC should be caused by Fe(IV) through oxygen/hydrogen atom transfer attack.

The TOC removal rate of the $FeTiO_3$/PS/light system for the treatment of 5 mg/L of TC is ca. 45% after 3 h light irradiation (Figure S13), demonstrating a comparatively mild mineralization ability of Fe(IV) species. The complete mineralization of TC can be achieved in the $FeTiO_3$/PS/dark system with a significantly improved PS concentration (40 mM), which should be attributed to the more aggressive sulfate and hydroxyl radicals. It seems that the degradation induced by Fe(IV) is much milder compared with that induced by sulfate and hydroxyl radicals. The selective mild degradation on the catalyst surface is expected to help alleviate the dilemma caused by the severe consumption of aggressive radicals by natural organic matters in real aqueous environment.

For the Fes/PS system, it is generally believed that $SO_4^{\cdot-}$ and $^{\cdot}OH$ are the dominant radicals that commonly coexist in the homogeneous or heterogeneous reaction. The latter is considered as the hydrolytic derivative of $SO_4^{\cdot-}$, particularly in highly alkaline conditions (pH > 10), where the base-activation of $S_2O_8^{2-}$ will also be involved.[42] Here, the pH for all of the reaction systems is controlled in the range of 4-10, and thus the evolution of $^{\cdot}OH$ can be neglected considering its low reaction rate compared with other evolution processes of $SO_4^{\cdot-}$. The reason for the negligible $SO_4^{\cdot-}$ and the formation of Fe(IV) in the $FeTiO_3$/PS/light system is inferred as follows. The decomposition of PS leads to the formation of $SO_4^{\cdot-}$ and Fe(III). $SO_4^{\cdot-}$ tends to be adsorbed by $FeTiO_3$ through complexing with the surficial iron species. The local concentration of Fe(II) around surficial $SO_4^{\cdot-}$ is thus increased. The adsorbed $SO_4^{\cdot-}$ is further consumed by Fe(II) and reduced to SO_4^{2-}, which accelerates the formation of Fe(III)-SO_4

353 complex on the $FeTiO_3$ surface. Under dark conditions, Fe(II) sites are shielded by the
354 surficial Fe(III)-SO_4 complex. This gives rise to the rapid deactivation of $FeTiO_3$ in the dark,
355 but is the key step for the formation of surface ≡Fe(IV) under visible light irradiation, which
356 can be further oxidized to Fe(IV) by the photo-generated hole.

357 **4. Conclusion**

358 In this work, the formation of Fe(IV) from a visible light-irradiated $FeTiO_3$/PS system is
359 clearly verified using PMSO as the probe. SO_4^{2-} decomposed *in situ* from PS plays a vital role
360 in the formation of surface Fe(IV) because its formation promotes the hole-electron separation
361 and it can form surface complex with Fe(III), which as an abundant species in PS-based
362 systems has long been neglected. The novel oxidative system with Fe(IV) as the active
363 species can be utilized for the selective removal of organic contaminants in complicated
364 wastewater matrices because of its unique reaction selectivity. The insignificant iron leaching
365 under acidic conditions benefitting from the stabilization effect of SO_4^{2-} makes the
366 $FeTiO_3$/PS/light system a strong candidate for acidic waste water treatment without the
367 second pollution. The effective activity in neutral to basic conditions further widens the range
368 of possible application conditions. $FeTiO_3$ is a stable mineral compound that is widely present
369 in rich ilmenite ores, a fact which is helpful for promoting the use of natural ores for
370 environment remediation. Moreover, sulfate ions are widely found in nature. The visible light
371 activity of the corresponding ≡$Fe(SO_4)_m$ complex further makes this system a robust candidate
372 for the *in situ* oxidation processes.

373 **Appendix A. Supplementary data**

374 The other supplementary details data to this article.

375 **Acknowledgements**

This work was supported by the National Natural Science Foundation of China (21673073, 21677048, 5171101651 and 21811540394), Shanghai Municipal Science and Technology Major Project (2018SHZDZX03), the Programme of Introducing Talents of Discipline to Universities (B20031, B16017), Shanghai Municipal Science and Technology (18520710200 and 17520711500) and the Fundamental Research Funds for the Central Universities and the Fundamental Research Funds for the Central Universities (222201717003).

L.P. and W.S. contributed equally to this work. The manuscript was written with contributions from all authors. All authors have approved the final version of the manuscript.

Conflict of Interst

The authors declare no competing financial interest.

Received: ((will be filled in by the editorial staff))
Revised: ((will be filled in by the editorial staff))
Published online: ((will be filled in by the editorial staff))

REFERENCES

[1] M. Xing, W. Xu, C. Dong, Y. Bai, J. Zeng, Y. Zhou, J. Zhang, Y. Yin, Metal Sulfides as Excellent Co-catalysts for H_2O_2 Decomposition in Advanced Oxidation Processes, Chem, 4 (2018) 1359-1372.
[2] H. Liu, T.A. Bruton, F.M. Doyle, D.L. Sedlak, In Situ Chemical Oxidation of Contaminated Groundwater by Persulfate: Decomposition by Fe(III)- and Mn(IV)-Containing Oxides and Aquifer Materials, Environmental Science & Technology, 48 (2014) 10330-10336.
[3] S.-Y. Oh, H.-W. Kim, J.-M. Park, H.-S. Park, C. Yoon, Oxidation of polyvinyl alcohol by persulfate activated with heat, Fe^{2+}, and zero-valent iron, Journal of Hazardous Materials, 168 (2009) 346-351.
[4] J.H. Ramirez, F.J. Maldonado-Hódar, A.F. Pérez-Cadenas, C. Moreno-Castilla, C.A. Costa, L.M. Madeira, Azo-dye Orange II degradation by heterogeneous Fenton-like reaction using carbon-Fe catalysts, Applied Catalysis B: Environmental, 75 (2007) 312-323.
[5] M.B. Kasiri, H. Aleboyeh, A. Aleboyeh, Degradation of Acid Blue 74 using Fe-ZSM5 zeolite as a heterogeneous photo-Fenton catalyst, Applied Catalysis B: Environmental, 84 (2008) 9-15.
[6] J. Feng, X. Hu, P.L. Yue, Novel Bentonite Clay-Based Fe−Nanocomposite as a Heterogeneous Catalyst for Photo-Fenton Discoloration and Mineralization of Orange II, Environmental Science & Technology, 38 (2004) 269-275.
[7] C. Xie, D. Cen, Z. Ren, Y. Wang, Y. Wu, X. Li, G. Han, X. Cai, FeS@BSA Nanoclusters to Enable H_2S-Amplified ROS-Based Therapy with MRI Guidance, Advanced Science, n/a (2020) 1903512.
[8] O. Pestovsky, S. Stoian, E.L. Bominaar, X. Shan, E. Münck, L. Que Jr, A. Bakac, Aqueous

FeIV=O: Spectroscopic Identification and Oxo-Group Exchange, Angewandte Chemie International Edition, 44 (2005) 6871-6874.
[9] S.-Y. Pang, J. Jiang, J. Ma, Oxidation of Sulfoxides and Arsenic(III) in Corrosion of Nanoscale Zero Valent Iron by Oxygen: Evidence against Ferryl Ions (Fe(IV)) as Active Intermediates in Fenton Reaction, Environmental Science & Technology, 45 (2011) 307-312.
[10] S. Gao, H. Lin, H. Zhang, H. Yao, Y. Chen, J. Shi, Nanocatalytic Tumor Therapy by Biomimetic Dual Inorganic Nanozyme-Catalyzed Cascade Reaction, Advanced Science, 6 (2019) 1801733.
[11] Q. Zhang, Q. Guo, Q. Chen, X. Zhao, S.J. Pennycook, H. Chen, Highly Efficient 2D NIR-II Photothermal Agent with Fenton Catalytic Activity for Cancer Synergistic Photothermal–Chemodynamic Therapy, Advanced Science, n/a (2020) 1902576.
[12] Z. Cao, L. Zhang, K. Liang, S. Cheong, C. Boyer, J.J. Gooding, Y. Chen, Z. Gu, Biodegradable 2D Fe–Al Hydroxide for Nanocatalytic Tumor-Dynamic Therapy with Tumor Specificity, Advanced Science, 5 (2018) 1801155.
[13] C. Dong, J. Ji, B. Shen, M. Xing, J. Zhang, Enhancement of H_2O_2 Decomposition by the Co-catalytic Effect of WS2 on the Fenton Reaction for the Synchronous Reduction of Cr(VI) and Remediation of Phenol, Environmental Science & Technology, 52 (2018) 11297-11308.
[14] H. Hori, Y. Nagaoka, M. Murayama, S. Kutsuna, Efficient decomposition of perfluorocarboxylic acids and alternative fluorochemical surfactants in hot water, Environ. Sci. Technol., 42 (2008) 7438-7443.
[15] M.G. Antoniou, A. Armah, D.D. Dionysiou, Degradation of microcystin-LR using sulfate radicals generated through photolysis, thermolysis and e− transfer mechanisms, Appl. Catal., B, 96 (2010) 290-298.
[16] A. Rastogi, S.R. Al-Abed, D.D. Dionysiou, Sulfate radical-based ferrous–peroxymonosulfate oxidative system for PCBs degradation in aqueous and sediment systems, Applied Catalysis B: Environmental, 85 (2009) 171-179.
[17] Y. Deng, C.M. Ezyske, Sulfate radical-advanced oxidation process (SR-AOP) for simultaneous removal of refractory organic contaminants and ammonia in landfill leachate, Water Research, 45 (2011) 6189-6194.
[18] Y.-H. Guan, J. Ma, Y.-M. Ren, Y.-L. Liu, J.-Y. Xiao, L.-q. Lin, C. Zhang, Efficient degradation of atrazine by magnetic porous copper ferrite catalyzed peroxymonosulfate oxidation via the formation of hydroxyl and sulfate radicals, Water Research, 47 (2013) 5431-5438.
[19] Y. Wang, J. Le Roux, T. Zhang, J.-P. Croué, Formation of Brominated Disinfection Byproducts from Natural Organic Matter Isolates and Model Compounds in a Sulfate Radical-Based Oxidation Process, Environmental Science & Technology, 48 (2014) 14534-14542.
[20] G. Fang, J. Gao, D.D. Dionysiou, C. Liu, D. Zhou, Activation of Persulfate by Quinones: Free Radical Reactions and Implication for the Degradation of PCBs, Environmental Science & Technology, 47 (2013) 4605-4611.
[21] G.P. Anipsitakis, D.D. Dionysiou, M.A. Gonzalez, Cobalt-Mediated Activation of Peroxymonosulfate and Sulfate Radical Attack on Phenolic Compounds. Implications of Chloride Ions, Environmental Science & Technology, 40 (2006) 1000-1007.
[22] G.P. Anipsitakis, T.P. Tufano, D.D. Dionysiou, Chemical and microbial decontamination of pool water using activated potassium peroxymonosulfate, Water Research, 42 (2008) 2899-2910.
[23] H.V. Lutze, S. Bircher, I. Rapp, N. Kerlin, R. Bakkour, M. Geisler, C. von Sonntag, T.C. Schmidt, Degradation of Chlorotriazine Pesticides by Sulfate Radicals and the Influence of Organic Matter, Environmental Science & Technology, 49 (2015) 1673-1680.
[24] G.P. Anipsitakis, D.D. Dionysiou, Radical Generation by the Interaction of Transition Metals with Common Oxidants, Environmental Science & Technology, 38 (2004) 3705-3712.

[25] Z. Wang, J. Jiang, S. Pang, Y. Zhou, C. Guan, Y. Gao, J. Li, Y. Yang, W. Qiu, C. Jiang, Is Sulfate Radical Really Generated from Peroxydisulfate Activated by Iron(II) for Environmental Decontamination?, Environmental Science & Technology, 52 (2018) 11276-11284.
[26] A. Ansari, A. Kaushik, G. Rajaraman, Mechanistic Insights on the ortho-Hydroxylation of Aromatic Compounds by Non-heme Iron Complex: A Computational Case Study on the Comparative Oxidative Ability of Ferric-Hydroperoxo and High-Valent FeIV=O and FeV=O Intermediates, Journal of the American Chemical Society, 135 (2013) 4235-4249.
[27] J. Park, Y. Morimoto, Y.-M. Lee, W. Nam, S. Fukuzumi, Metal Ion Effect on the Switch of Mechanism from Direct Oxygen Transfer to Metal Ion-Coupled Electron Transfer in the Sulfoxidation of Thioanisoles by a Non-Heme Iron(IV)−Oxo Complex, Journal of the American Chemical Society, 133 (2011) 5236-5239.
[28] O. Pestovsky, A. Bakac, Reactivity of Aqueous Fe(IV) in Hydride and Hydrogen Atom Transfer Reactions, Journal of the American Chemical Society, 126 (2004) 13757-13764.
[29] X. Lang, X. Chen, J. Zhao, Heterogeneous visible light photocatalysis for selective organic transformations, Chemical Society Reviews, 43 (2014) 473-486.
[30] X. Cheng, H. Guo, Y. Zhang, Y. Liu, H. Liu, Y. Yang, Oxidation of 2,4-dichlorophenol by non-radical mechanism using persulfate activated by Fe/S modified carbon nanotubes, Journal of Colloid and Interface Science, 469 (2016) 277-286.
[31] Y.J. Kim, B. Gao, S.Y. Han, M.H. Jung, A.K. Chakraborty, T. Ko, C. Lee, W.I. Lee, Heterojunction of $FeTiO_3$ nanodisc and TiO_2 nanoparticle for a novel visible light photocatalyst, The Journal of Physical Chemistry C, 113 (2009) 19179-19184.
[32] P. Bilski, K. Reszka, M. Bilska, C.F. Chignell, Oxidation of the Spin Trap 5, 5-Dimethyl-1-pyrroline N-Oxide by Singlet Oxygen in Aqueous Solution, Journal of the American Chemical Society, 118 (1996) 1330-1338.
[33] X. Zhang, M. Feng, R. Qu, H. Liu, L. Wang, Z. Wang, Catalytic degradation of diethyl phthalate in aqueous solution by persulfate activated with nano-scaled magnetic $CuFe_2O_4$/MWCNTs, Chemical Engineering Journal, 301 (2016) 1-11.
[34] M. Feng, R. Qu, X. Zhang, P. Sun, Y. Sui, L. Wang, Z. Wang, Degradation of flumequine in aqueous solution by persulfate activated with common methods and polyhydroquinone-coated magnetite/multi-walled carbon nanotubes catalysts, Water Research, 85 (2015) 1-10.
[35] G. Fang, C. Liu, J. Gao, D.D. Dionysiou, D. Zhou, Manipulation of Persistent Free Radicals in Biochar to Activate Persulfate for Contaminant Degradation, Environmental Science & Technology, 49 (2015) 5645-5653.
[36] C. S. Turchi, D. F. Ollis, Photocatalytic degradation of organic water contaminants: Mechanisms involving hydroxyl radical attack, Journal of Catalysis, 122 (1990) 178-192.
[37] P. Hu, H. Su, Z. Chen, C. Yu, Q. Li, B. Zhou, P.J.J. Alvarez, M. Long, Selective Degradation of Organic Pollutants Using an Efficient Metal-Free Catalyst Derived from Carbonized Polypyrrole via Peroxymonosulfate Activation, Environmental Science & Technology, 51 (2017) 11288-11296.
[38] H. Li, C. Shan, B. Pan, Fe(III)-Doped g-C_3N_4 Mediated Peroxymonosulfate Activation for Selective Degradation of Phenolic Compounds via High-Valent Iron-Oxo Species, Environmental Science & Technology, 52 (2018) 2197-2205.
[39] H. Wang, H. Yao, P. Sun, D. Li, C.-H. Huang, Transformation of Tetracycline Antibiotics and Fe(II) and Fe(III) Species Induced by Their Complexation, Environmental Science & Technology, 50 (2016) 145-153.
[40] M.A. Ghandour, H.A. Azab, A. Hassan, A.M. Ali, Potentiometric studies on the complexes of tetracycline (TC) and oxytetracyclin (OTC) with some metal ions, Monatshefte für Chemie / Chemical Monthly, 123 (1992) 51-58.
[41] Z. Xie, Y. Feng, F. Wang, D. Chen, Q. Zhang, Y. Zeng, W. Lv, G. Liu, Construction of carbon dots modified MoO_3/g-C_3N_4 Z-scheme photocatalyst with enhanced visible-light

photocatalytic activity for the degradation of tetracycline, Applied Catalysis B: Environmental, 229 (2018) 96-104.
[42] G.-X. Huang, C.-Y. Wang, C.-W. Yang, P.-C. Guo, H.-Q. Yu, Degradation of Bisphenol A by Peroxymonosulfate Catalytically Activated with $Mn_{1.8}Fe_{1.2}O_4$ Nanospheres: Synergism between Mn and Fe, Environmental Science & Technology, 51 (2017) 12611-12618.
[43] K. Xu, W. Ben, W. Ling, Y. Zhang, J. Qu, Z. Qiang, Impact of humic acid on the degradation of levofloxacin by aqueous permanganate: Kinetics and mechanism, Water Research, 123 (2017) 67-74.
[44] I. Yamazaki, L.H. Piette, EPR Spin-Trapping Study on the Oxidizing Species Formed in the Reaction of the Ferrous Ion with Hydrogen Peroxide, Journal of the American Chemical Society, 113 (1991) 7588-7593.
[45] B. Shao, H. Dong, B. Sun, X. Guan, Role of Ferrate(IV) and Ferrate(V) in Activating Ferrate(VI) by Calcium Sulfite for Enhanced Oxidation of Organic Contaminants, Environmental Science & Technology, 53 (2019) 894-902.
[46] O. Pestovsky, A. Bakac, Aqueous Ferryl(IV) Ion: Kinetics of Oxygen Atom Transfer To Substrates and Oxo Exchange with Solvent Water, Inorganic Chemistry, 45 (2006) 814-820.
[47] H. Bataineh, O. Pestovsky, A. Bakac, pH-induced mechanistic changeover from hydroxyl radicals to iron(IV) in the Fenton reaction, Chemical Science, 3 (2012) 1594-1599.
[48] W.W. Rudolph, G. Irmer, G.T. Hefter, Raman spectroscopic investigation of speciation in $MgSO_4$(aq), Physical Chemistry Chemical Physics, 5 (2003) 5253-5261.
[49] J.M. Dudik, C.R. Johnson, S.A. Asher, Wavelength dependence of the preresonance Raman cross sections of CH_3CN, SO_4^{2-}, ClO_4^-, and NO_3^-, The Journal of Chemical Physics, 82 (1985) 1732-1740.
[50] J.-L. Dong, X.-H. Li, L.-J. Zhao, H.-S. Xiao, F. Wang, X. Guo, Y.-H. Zhang, Raman Observation of the Interactions between NH_4^+, SO_4^{2-}, and H_2O in Supersaturated $(NH_4)_2SO_4$ Droplets, The Journal of Physical Chemistry B, 111 (2007) 12170-12176.
[51] X. Guo, H.-S. Xiao, F. Wang, Y.-H. Zhang, Micro-Raman and FTIR Spectroscopic Observation on the Phase Transitions of $MnSO_4$ Droplets and Ionic Interactions between Mn^{2+} and SO_4^{2-}, The Journal of Physical Chemistry A, 114 (2010) 6480-6486.
[52] H. Liu, P. Sun, M. Feng, H. Liu, S. Yang, L. Wang, Z. Wang, Nitrogen and sulfur co-doped CNT-COOH as an efficient metal-free catalyst for the degradation of UV filter BP-4 based on sulfate radicals, Applied Catalysis B: Environmental, 187 (2016) 1-10.
[53] J. Du, J. Bao, X. Fu, C. Lu, S.H. Kim, Facile preparation of S/Fe composites as an effective peroxydisulfate activator for RhB degradation, Separation and Purification Technology, 163 (2016) 145-152.
[54] J. Zhu, W. Zheng, B. He, J. Zhang, M. Anpo, Characterization of Fe–TiO_2 photocatalysts synthesized by hydrothermal method and their photocatalytic reactivity for photodegradation of XRG dye diluted in water, Journal of Molecular Catalysis A: Chemical, 216 (2004) 35-43.
[55] J. Zhu, F. Chen, J. Zhang, H. Chen, M. Anpo, Fe^{3+}-TiO_2 photocatalysts prepared by combining sol–gel method with hydrothermal treatment and their characterization, Journal of Photochemistry and Photobiology A: Chemistry, 180 (2006) 196-204.
[56] X. Lv, D.Y.S. Yan, F.L.-Y. Lam, Y.H. Ng, S. Yin, A.K. An, Solvothermal synthesis of copper-doped BiOBr microflowers with enhanced adsorption and visible-light driven photocatalytic degradation of norfloxacin, Chemical Engineering Journal, 401 (2020) 126012.
[57] Y. Ji, Y. Shi, W. Dong, X. Wen, M. Jiang, J. Lu, Thermo-activated persulfate oxidation system for tetracycline antibiotics degradation in aqueous solution, Chemical Engineering Journal, 298 (2016) 225-233.
[58] Z. Ma, L. Hu, X. Li, L. Deng, G. Fan, Y. He, A novel nano-sized MoS_2 decorated Bi_2O_3 heterojunction with enhanced photocatalytic performance for methylene blue and tetracycline degradation, Ceramics International, 45 (2019) 15824-15833.
[59] Y. Yang, Z. Zeng, C. Zhang, D. Huang, G. Zeng, R. Xiao, C. Lai, C. Zhou, H. Guo, W.

Xue, M. Cheng, W. Wang, J. Wang, Construction of iodine vacancy-rich BiOI/Ag@AgI Z-scheme heterojunction photocatalysts for visible-light-driven tetracycline degradation: Transformation pathways and mechanism insight, Chemical Engineering Journal, 349 (2018) 808-821.
[60] J. Wang, D. Zhi, H. Zhou, X. He, D. Zhang, Evaluating tetracycline degradation pathway and intermediate toxicity during the electrochemical oxidation over a Ti/Ti_4O_7 anode, Water Research, 137 (2018) 324-334.

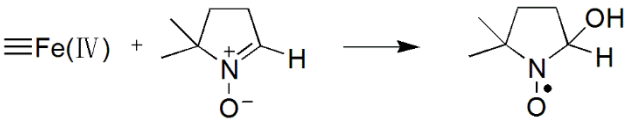

Fe(Ⅳ) DMPO DMPO-OH

Scheme 1. DMPO-•OH derived from the oxidation of DMPO by Fe(IV) through direct oxidation.

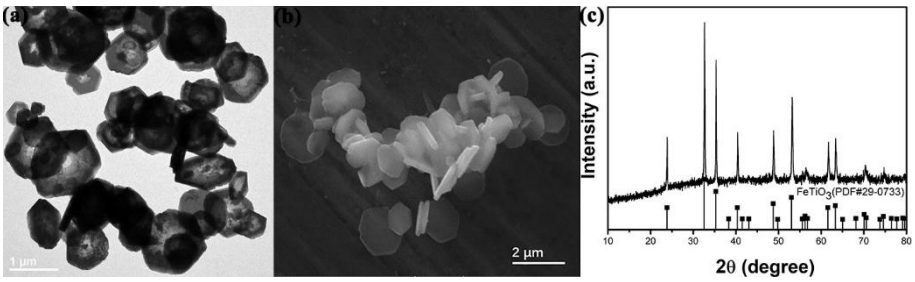

Figure 1. (a) TEM image, (b) SEM image and (c) XRD patterns of $FeTiO_3$.

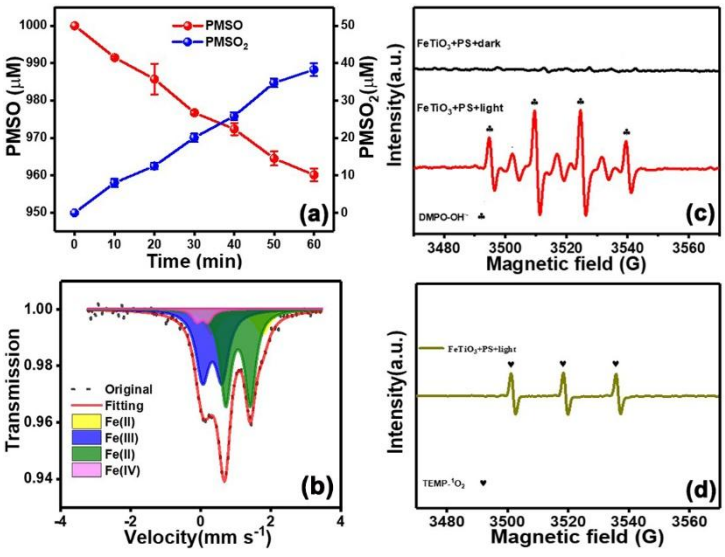

Figure 2. (a) Oxidation of PMSO and production of $PMSO_2$ in $FeTiO_3$/PS/light system (pH=4); (b) Mossbauer spectrum of recycled $FeTiO_3$ from the $FeTiO_3$/PS/Light system; (c) EPR spectra of the DMPO adduct formed from the $FeTiO_3$/PS/light and $FeTiO_3$/PS/dark

583 systems; (d) EPR spectrum of TEMP-$^1O_2$ formed from the $FeTiO_3$/PS/light system. (Cat.: 0.1

584 $g \cdot L^{-1}$, PS: 1 mM, DMPO: 0.1 mM, TEMP: 0.1 mM, reaction time: 20 min).

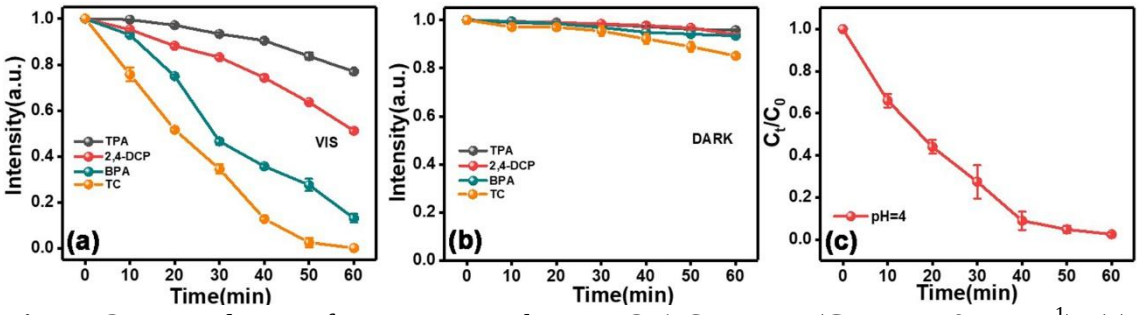

585

586 **Figure 3.** Degradation of aromatics in the $FeTiO_3$/PS system (C_{FeTiO3} = 0.1 $g \cdot L^{-1}$): (a) under

587 the visible light irradiation; (b) in the dark. The TC concentration is 20 mg/L and the

588 corresponding PS concentration is 2 mM. For other reactions, the aromatics concentration is

589 fixed at 10 mg/L and the PS concentration is 5 mM; (c) Influence of pH buffer solution on TC

590 degradation (Cat.: 0.1 $g \cdot L^{-1}$, TC: 20 $mg \cdot L^{-1}$, PS: 2 mM).

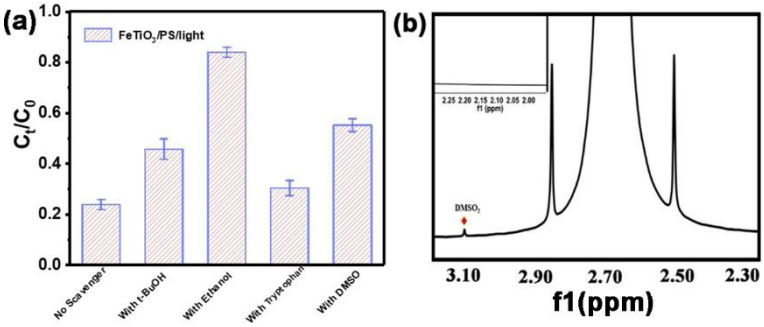

591

592 **Figure 4.** (a) Performances of the $FeTiO_3$/PS/light system with different scavengers (Cat.: 0.1

593 $g \cdot L^{-1}$, TC: 20 $mg \cdot L^{-1}$, PS: 1 mM, TBA: 100 mM, ethanol: 100 mM, tryptophan: 10 mg and

594 DMSO: 100 mM, initial pH = 4); (b) ^1H NMR spectrum of the product obtained in D_2O (0.2

595 g/L of $FeTiO_3$, 2 mM of PS, 10 mL of DMSO, light). The $DMSO_2$ peak is denoted by a

596 diamond.

597 **.** DMPO-•OH derived from the oxidation of DMPO by Fe(IV) through direct oxidation.

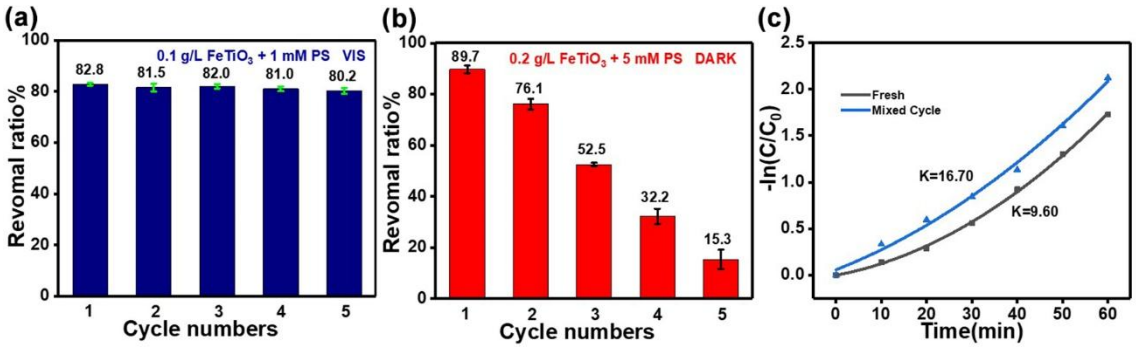

Figure 5. (a) Cyclic performance of the $FeTiO_3$/PS/light system (Cat.: 0.1 g·L^{-1}, TC: 20 mg·L^{-1}, PS: 1 mM); (b) Cyclic performance of the $FeTiO_3$/PS/dark system (Cat.: 0.2 g·L^{-1}, TC: 20 mg·L^{-1}, PS: 5 mM); (c) The simulated reaction kinetics of the fresh sample and the deactivated sample recycled from 5-run dark reaction.

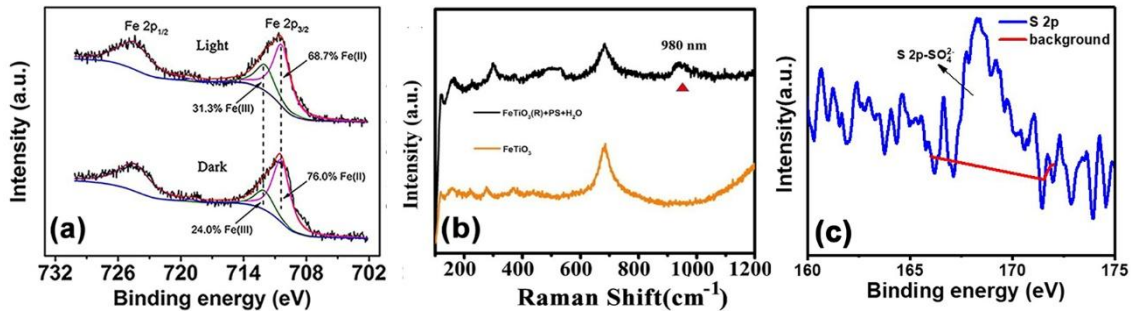

Figure 6. (a) XPS spectra for Fe 2p regions of $FeTiO_3$ in light and dark systems; XPS spectra of $FeTiO_3$ after dark reaction (b) S 2p; (c) Raman spectra of the $FeTiO_3$ before and after reaction.

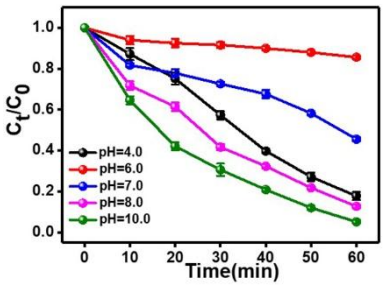

Figure 7. Influence of pH on the TC degradation efficiency of the $FeTiO_3$/PS/light system (Cat.: 0.1 g·L^{-1}, TC: 20 mg·L^{-1}, PS: 1 mM).

Graphical abstract

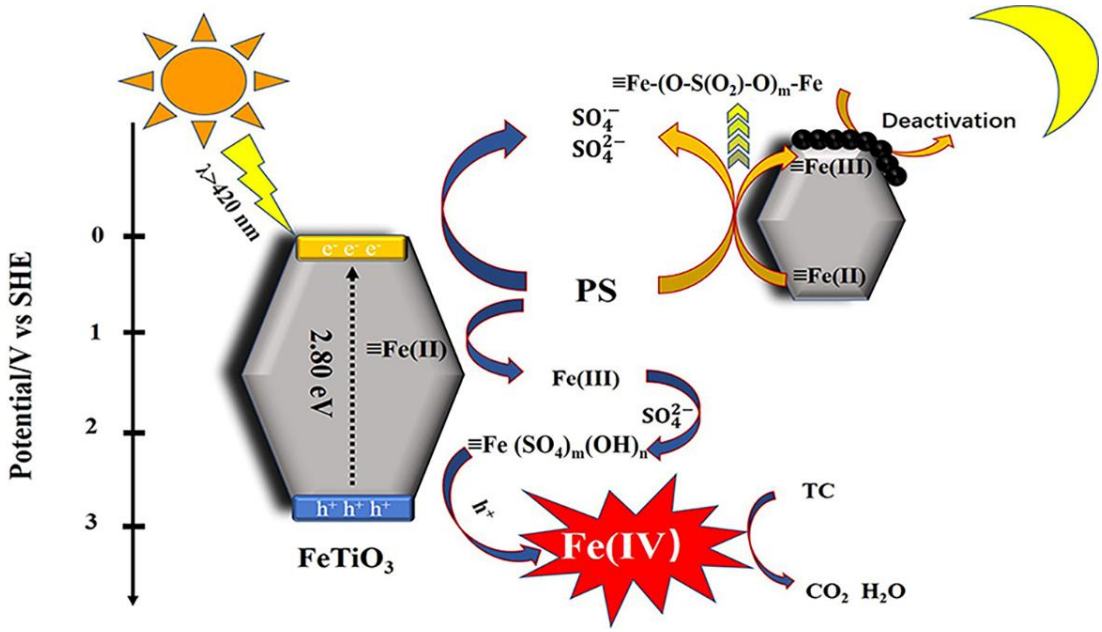

The in situ formed surficial Fe(III)-SO_4 complex causes the deactivation of $FeTiO_3$/PS system under the dark conditions, which however is the key intermediate for the further evolution to Fe(IV) species by photo-induced hole under the visible light irradiation. Selective and recyclable degradation of aromatics with higher ionization potential can be achieved over Fe(IV) formed from the $FeTiO_3$/PS/light system.

Highlights

- The $FeTiO_3$/PS system shows selectively photocatalytic performance towards phenolics
- A complex is in situ formed from Fe(III) and SO_4^{2-} on the FeTiO3 surface
- The complex is the key intermediate for Fe(IV) production
- The photo-generated high-valent Fe(IV) is responsible for the selective degradation

Supplementary Material

Click here to download Supplementary Material: ACB article-SI final.docx